Available online at www.sciencedirect.com

ScienceDirect

Ceramics International 42 (2016) 3145–3153

CERAMICS INTERNATIONAL

www.elsevier.com/locate/ceramint

Performance of $La_{0.6}Sr_{0.4}Co_{1-y}Fe_yO_3$ ($y=0.2$, 0.5 and 0.8) nanostructured cathodes for intermediate-temperature solid-oxide fuel cells: Influence of microstructure and composition

Augusto Mejía Gómez[a,b,c], Joaquín Sacanell[a,b], Ana Gabriela Leyva[a,c], Diego G. Lamas[b,c,*]

[a]*Departamento de Física de la Materia Condensada, Gerencia de Investigación y Aplicaciones, Centro Atómico Constituyentes, Comisión Nacional de Energía Atómica, Av. General Paz 1499, 1650 Buenos Aires, Argentina*

[b]*CONICET, Argentina*

[c]*Escuela de Ciencia y Tecnología, Universidad Nacional de General San Martín, Martín de Irigoyen 3100, Edificio Tornavía, Campus Miguelete, 1650 San Martín, Pcia. de Buenos Aires, Argentina*

Received 14 September 2015; received in revised form 20 October 2015; accepted 21 October 2015
Available online 27 October 2015

Abstract

We investigated the electrochemical properties of Co–Fe perovskites, which can be used as cathodes for intermediate-temperature solid-oxide fuel cells (IT-SOFCs). We studied the electrochemical properties of nanostructured mixed ionic-electronic conductors for IT-SOFC cathodes with compositions of $La_{0.6}Sr_{0.4}Co_{1-y}Fe_yO_3$ ($y=0.2$, 0.5 and 0.8). We analyzed the performance of two types of nanostructures: nanorods and nanotubes. Our results show that the electrochemical performance is highly influenced by the form of nanostructure, whereas the effect of composition is less significant.

© 2015 Elsevier Ltd and Techna Group S.r.l. All rights reserved.

Keywords: SOFC; Nanostructured cathodes; Nanotubes; Nanorods

1. Introduction

Fuel cells, which convert chemical energy directly into electrical energy, are one of the most promising devices for large-scale environmentally clean power generation [1–3]. Among the fuel cell types, solid-oxide fuel cells (SOFCs) have the advantage of allowing the use of different fuels, such as hydrogen or hydrocarbons. However, the typical operating temperature of SOFCs is approximately 1000 °C, leading to degradation of the composing materials. Thus, significant effort has been devoted to decreasing the operating temperature of these devices to produce intermediate-temperature SOFCs (IT-SOFCs) that operate at 500–700 °C, thereby avoiding degradation problems due to thermal cycling or diffusion at the interfaces and reducing the cost of the interconnection materials [2,4,5].

Nanostructured materials have recently attracted great interest due to their new and/or enhanced properties. For this reason, fabrication of nanostructures using different materials and methods is a rapidly growing field of interdisciplinary research. Nanostructures displaying a wide variety of useful properties have been developed in recent years [6–8]. Carbon nanotubes and semiconductor and metallic nanowires are of interest for their optical and electronic properties. In the case of SOFCs, the novel properties of such nanostructures have improved the performance of cathodes [9–13], anodes [14] and electrolytes [15–17]. These nanostructures have already been used in power generation devices, such as lithium-ion batteries [18,19] and other energy and storage devices [20]. In conventional SOFCs, which operate at ~1000 °C, the use of nanostructured materials has not been pursued because grain growth is expected to occur at such high temperatures. However, the use of nanostructured materials in IT-SOFCs is possible

*Corresponding author at: Escuela de Ciencia y Tecnología, Universidad Nacional de General San Martín, Martín de Irigoyen 3100, Edificio Tornavía, Campus Miguelete, 1650 San Martín, Pcia. de Buenos Aires, Argentina. Tel.: +541167727657.

E-mail address: diego_german_lamas@yahoo.com.ar (D.G. Lamas).

http://dx.doi.org/10.1016/j.ceramint.2015.10.104
0272-8842/© 2015 Elsevier Ltd and Techna Group S.r.l. All rights reserved.

because grain growth can be minimized at the lower operating temperature range.

Nanostructured cathodes based on mixed ionic/electronic conductors (MIECs) are particularly interesting because the number of active sites for the oxygen reduction is expected to increase dramatically due to the increase in the specific surface area. Fig. S1 of the Supplementary material [21] shows a schematic representation of the processes occurring in MIEC cathodes. Oxygen can be adsorbed onto the entire cathode surface and dissociate. As a result, electrons can reduce oxygen to form oxide ions that subsequently reach the electrolyte through ionic conduction across the cathode volume. However, the increase in the specific surface area is not the only factor that could potentially enhance the cathodes performance. As mentioned above, ionic conduction has been demonstrated to increase in both electrolytes [15,16] and cathodes [9,11]. This enhancement is due to the emergence of a significant influence of grain boundary anion conduction in nanostructured materials.

Recently, the synthesis of nanotubes and nanowires of perovskite-type mixed oxides has been investigated. For example, the synthesis of rare-earth manganese mixed oxide nanotubes via a pore wetting technique [22,23] and the hydrothermal synthesis of single-crystal $La_{0.5}Sr_{0.5}MnO_3$ nanowires [24] have been reported. Because these nanostructures have a high specific surface area, they have been proposed for use in SOFC cathodes [25]. However, manganites typically have low catalytic activity for oxygen reduction at intermediate temperatures [4,26,27]. For this reason, most of the research studies on nanostructured cathodes for SOFCs are focused on MIEC materials. Note that this focus on MIEC materials does not mean that it is not worth studying nanostructured LSM cathodes. In fact, our group is currently studying nanostructured manganites to understand how to improve their performance as a cathode operating in the temperature range of 700–800 °C.

In previous works, we presented a new type of highly porous nanostructured cathodes that exhibit very low polarization resistance; such cathodes were prepared from $La_{0.6}Sr_{0.4}CoO_3$ (LSC) nanotubes, following a very simple procedure [10,11]. The obtained cathodes showed significantly lower polarization resistance than that corresponding to microstructured cathodes, making these nanostructured cathodes good candidates for IT-SOFCs cathodes. We used tubular structures of submicrometric diameter formed by assembled nanoparticles. A detailed description of the synthesis procedure can be found elsewhere [22,23]. Similar improved performance has been obtained on several nanostructured SOFC cathodes [9,12,13]. We showed that the smaller the diameter of the precursor nanotubes is, the better are its electrochemical properties, in particular, the best performance was obtained for nanorods [11]. In addition, we observed that if nanotubes or nanorods are formed by smaller particles, then the bulk diffusion of oxide ions is improved. This improved ionic conduction is reminiscent to that observed in nanostructured electrolytes, in which it has been shown that fast grain boundary ion conduction is responsible for that behavior [15–17].

Table 1
Average particle sizes determined from SEM observations for all of the cathodes.

Cathode	Particle size (nm)	Cathode	Particle size (nm)
LSCF(0.2 – 2)	138	LSCF(0.2 – 8)	147
LSCF(0.5 – 2)	142	LSCF(0.5 – 8)	111
LSCF(0.8 – 2)	137	LSCF(0.8 – 8)	144

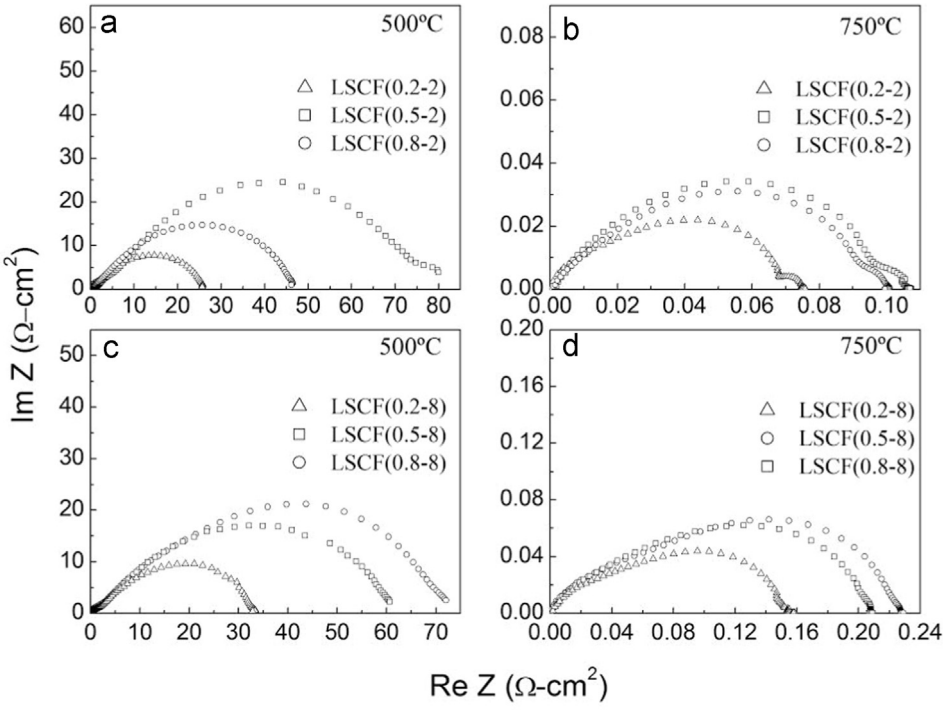

Fig. 1. Electrochemical Impedance Spectroscopy data for the LSCF($y-2$) cathode in air at (a) 500 °C and (b) 750 °C; for the LSCF($y-8$) cathode in air at (c) 500 °C and (d) 750 °C.

The partial substitution of Fe instead of Co is generally used to induce long-term stability of this material under operating conditions. Because we have been able to obtain $La_{0.6}Sr_{0.4}Co_{0.2}Fe_{0.8}O_3$ nanotubes [28], we propose here to extend our study of the electrochemical properties of $La_{0.6}Sr_{0.4}Co_{1-y}Fe_yO_3$ nanotubes as a function of the partial substitution of Co by Fe. We analyze the effect of the microstructure by using precursors of different diameter, and the effect of composition by varying the partial substitution of Co by Fe.

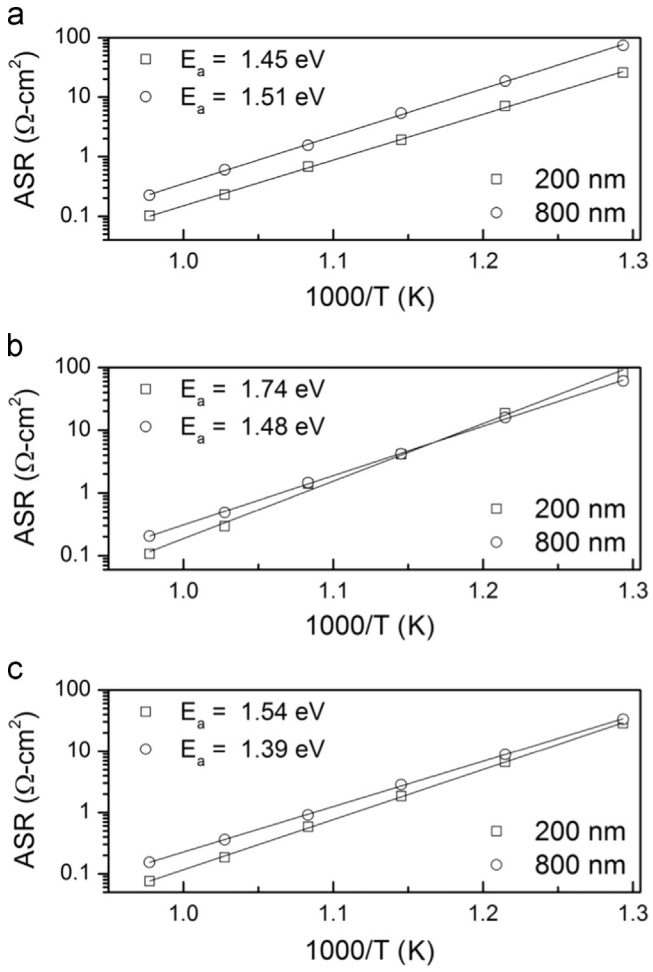

Fig. 2. Arrhenius plot of ASR for all cathodes in air. (a) LSCF(0.8−n), (b) LSCF(0.5−n) and (c) LSCF(0.2−n) (200 nm: rod-like nanostructure; 800 nm: tubular nanostructure).

Table 2
ASR and E_a values for LSCF($y-n$) cathodes.

Cathode	ASR (Ω cm²)		E_a(eV)
	750 °C	500 °C	
LSCF(0.2–2)	0.08	28.5	1.54
LSCF(0.2–8)	0.15	33.3	1.39
LSCF(0.5–2)	0.11	80.7	1.74
LSCF(0.5–8)	0.20	60.5	1.48
LSCF(0.8–2)	0.10	25.8	1.45
LSCF(0.8–8)	0.22	73.7	1.51

2. Materials and methods

To obtain $La_{0.6}Sr_{0.4}Co_{1-y}Fe_yO_3$ (LSCF), 1 M stoichiometric nitric solutions were prepared by dissolution of $Sr(NO_3)_2$, $La(NO_3)_3 6H_2O$, $Co(NO_3)_2 6H_2O$ and $Fe(NO_3)_3 9H_2O$ in pure water. All reagents were purchased from Merck, Germany (99.99% purity). Templates of porous polycarbonate films were used as filters in an adequate system for syringe filtration to ensure that the total volume of the pores was filled. Porous polycarbonate films were commercial Isopore™ membrane filters from Millipore. Membranes with pore sizes of 200 nm and 800 nm were used as templates and filled with a nitrate precursor solution. The membranes were further treated under microwave radiation for a few minutes and then calcined at 900 °C for 10 min, obtaining the desired perovskite structure, as confirmed by X-ray diffraction. Nanostructured samples calcined at 900 °C exhibited a crystallite size of approximately 30 nm. A detailed description of the synthesis procedure can be found in [11,22,27]. The samples and cathodes will be hereafter referred to as LSCF($y-n$), where y denotes the Fe doping, and $n=2$ and 8 for the cathodes made with membranes with pore size of 200 nm and 800 nm, respectively.

The compositions of the samples were confirmed using the Rutherford backscattering spectrometry (RBS) technique. These experiments were performed at Laboratório de Materiais e Feixes Iônicos (LAMFI), Instituto de Física, Universidade de São Paulo, Brazil using a He^+ beam with energy of $E=3.05$ MeV. RBS data were analyzed through the SIMNRA code. The results of this study are included in the Supplementary material [21], where it can be observed that they are close to those expected according to their nominal compositions.

X-ray powder diffraction was performed on the D10B-XPD line of the Brazilian Synchrotron Light Laboratory (LNLS, Campinas, Brazil), using a high-intensity configuration (low resolution) and a wavelength of 1.61017 Å.

The morphologies of the LSCF nanomaterials were examined via scanning electron microscopy (SEM) using a FEI Quanta 200 instrument (Laboratorio de Microscopia Electrónica, Laboratorio de Microscopía Electrónica, Unidad de Actividad de Materiales, Centro Atómico Constituyentes, CNEA, Argentina) and a FEI QUANTA 250 (Centro de investigación y desarrollo en mecánica, INTI, Argentina).

Electrolytes were prepared from commercial $Ce_{0.8}Gd_{0.2}O_{1.9}$ powders (GDC, Nextech Materials™) by uniaxial pressing at 200 MPa and sintering at 1350 °C for 3 h, obtaining 0.6 mm thick samples with a relative density higher than 96%. The density of the electrolytes was determined from their mass and dimensions and compared with the theoretical density of this material (7.23 g cm^{-3}). GDC was selected to compare our results with those reported in the literature because it is the most commonly used electrolyte.

LSCF nanomaterials were made into an ink for cathode deposition, using a commercial ink vehicle (IV) from Nextech Materials™. We tested different LSCO/IV mass ratios to obtain the best film adherence. We made inks for all of the samples, using a 1:2 LSCF:IV mass ratio in all cases, to optimize the viscosity of the ink and also to make equivalent samples for comparison. We painted several samples with the ink made by each of our powders

to check the reproducibility and also to compare the different procedures described above. Next, we smeared this ink with a brush on both sides of the electrolyte to fabricate symmetrical [LSCF/GDC/LSCF] cells. Once painted, the samples were dried at 50 °C in air for approximately 20 min. Afterwards, a conventional sintering of 1 h at 1000 °C, with a heating and cooling rate of 10 °C min^{-1} was conducted to attach the cathode to the electrolyte. The electrode area was approximately 0.2 cm^2.

The Area-Specific Resistance (ASR) of the cathodes was determined from Electrochemical Impedance Spectroscopy (EIS) measurements using a Metrohm Autolab PGSTAT 302 N potentiostat-galvanostat with an FRA module (CINSO-CONICET-CITEDEF, Argentina) in the frequency range from 0.02 Hz to 1 MHz with an excitation voltage of 20 mV. The performance for temperatures between 500 and 750 °C was analyzed. Pt paste was used as the current collector. The measurements were performed at zero bias. Under these conditions, our results were found to be highly reproducible. EIS measurements were performed in air, in pure oxygen and in a mixture of 95% of N_2 and 5% of O_2.

3. Results and discussion

The XRD patterns for all of the precursor nanostructures studied in this work are presented in Fig. S2 of the Supplementary material [21]. A pure perovskite-type phase with rhombohedral crystal structure was found for all samples. The nanocrystalline nature of the samples is evidenced by the broadening of Bragg peaks. The average crystallite size, estimated by the Scherrer equation, is approximately 30 nm for all samples.

The LSCF($y-2$) samples exhibit a rod-like nanostructure, while the LSCF($y-8$) display a tubular morphology. In both cases, those morphologies are a consequence of the agglomeration of the nanoparticles, and a porous structure was observed. SEM

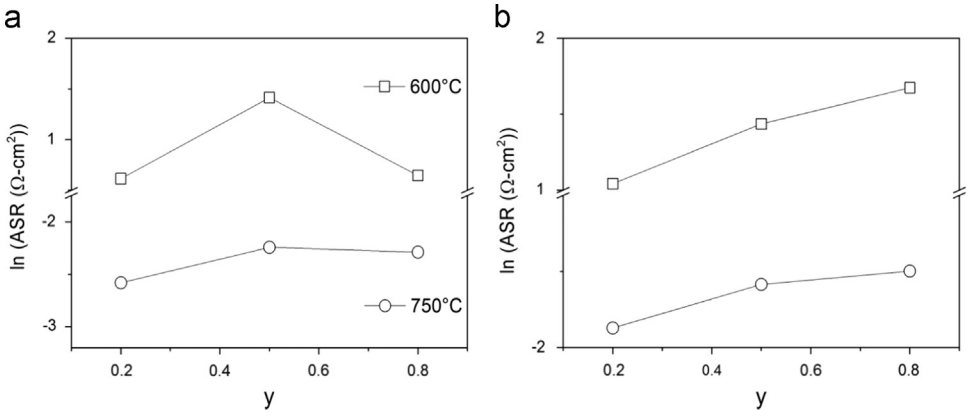

Fig. 3. ASR of LSCF($y-n$) cathodes as a function of Fe content: (a) cathodes with rod nanostructure (prepared using membranes with pores of 200 nm diameter) and (b) cathodes with tubular nanostructure (membranes with pores of 800 nm diameter).

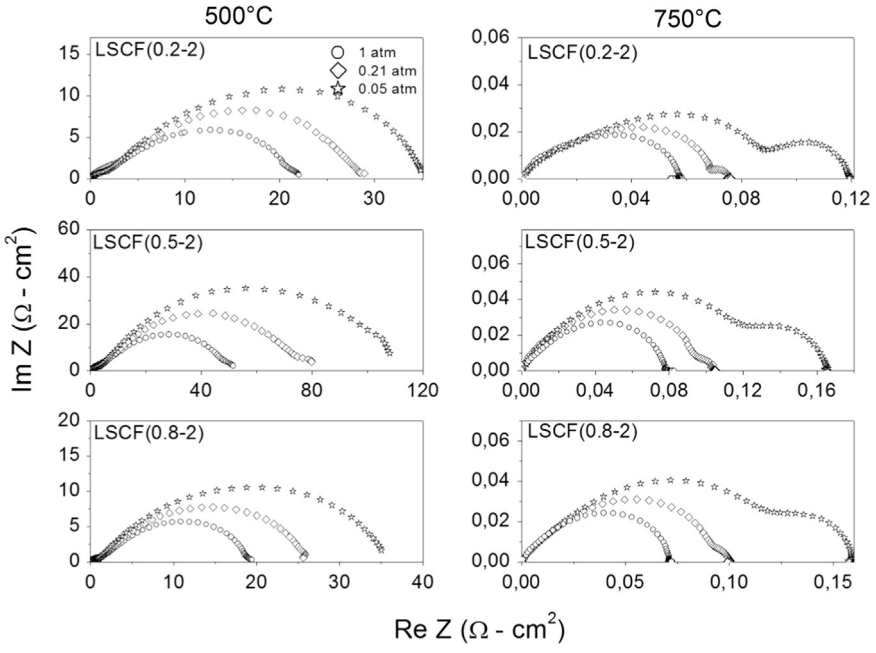

Fig. 4. Electrochemical Impedance Spectroscopy data for the LSCF($y-2$) cathodes under different oxygen partial pressures and temperatures.

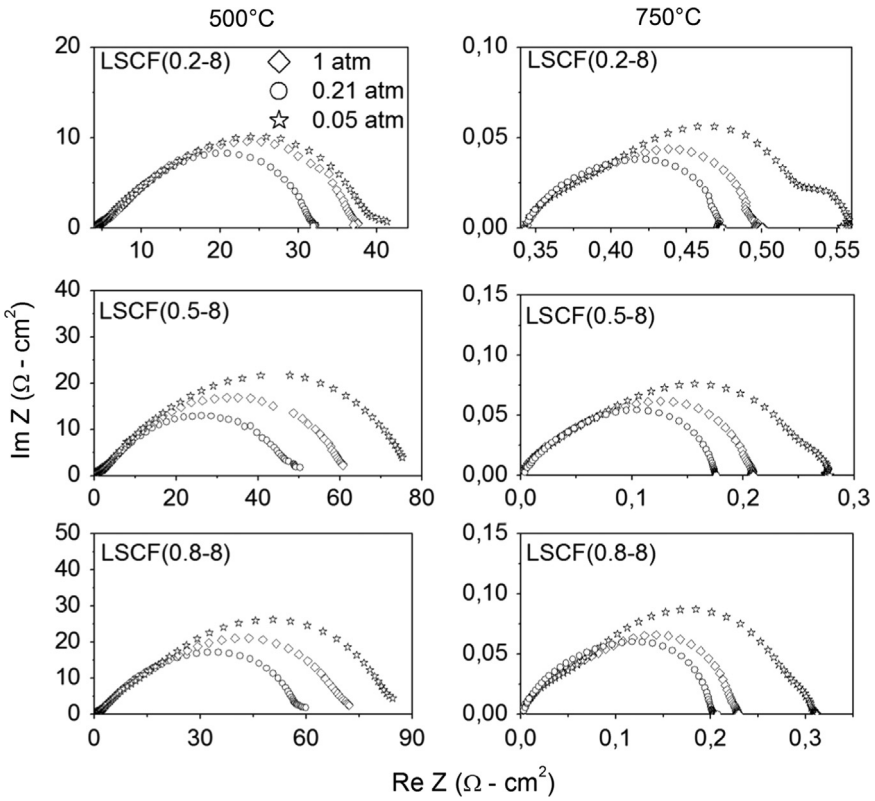

Fig. 5. Electrochemical Impedance Spectroscopy data for the LSCF($y-8$) cathodes under different oxygen partial pressures and temperatures.

Table 3
ASR values for LSCF(0.2 – 2) and LSCF(0.2 – 8) cathodes in different atmospheres.

Cathode	$p(O_2)$ (atm)	ASR (Ω cm^2)			
		750 °C	650 °C	600 °C	500 °C
LSCF(0.2 – 2)	1	0.06	0.49	1.52	22.08
	0.21	0.08	0.58	1.85	28.47
	0.05	0.12	0.69	2.14	34.97
LSCF(0.2 – 8)	1	0.13	0.80	2.42	27.88
	0.21	0.15	0.90	2.84	33.34
	0.05	0.22	1.11	3.44	37.12

micrographs of LSCF($y-2$) and LSCF($y-8$) samples are shown in Fig. S3(a) of the Supplementary material [21]. The morphology of the cathodes (i.e., after the sintering procedure) do not depend on composition but do depend on the average pore size of the membranes used in the synthesis route (see Fig. S3(b) and (c) of the Supplementary material [21]). The nanostructure of the material is retained after performing the sintering procedure, even though grain size growth is observed. The average sizes, determined from SEM observations for all of the cathodes, are summarized in Table 1.

Fig. 1(a) and (b), show the imaginary part vs. the real part of the impedance, i.e., the Nyquist plots, for the LSCF(0.2–2), LSCF(0.5–2) and LSCF(0.8–2) cathodes, measured at 500 °C and 750 °C in air, respectively. By this technique, processes with different characteristic times can be separated. All EIS spectra show a dominant impedance arc. The frequency always increases from right to left. We observed that in the LSCF ($y-2$) cathodes (those made with nanotubes of 200 nm of diameter), a low frequency component starts to develop at 700 °C, which is evident at 750 °C.

Fig. 1(c) and (d) show the EIS data corresponding to the LSCF($y-8$) cathodes, made with nanotubes of diameter of 800 nm. We can see an overall similar behavior, but the low frequency contribution, evident for the LSCF(y-2) cathodes, is practically absent. We will return to this result after performing a detailed analysis of the different contributions to the impedance as a function of the oxygen partial pressure ($p(O_2)$).

An indication of the cathode performance that can be obtained from EIS data is the ASR value, defined as the difference between the low frequency and the high frequency interceptions of the curves with the real axis. A lower ASR corresponds to an improved performance. We see that cathodes with lower Fe content exhibit improved electrochemical response, reaching the lowest ASR values compared with the other compositions. As a reference, an ASR of 0.07 Ω cm^2 is obtained for the cathode with rod-like nanostructure at 750 °C and 0.15 Ω cm^2 for the cathode prepared with nanotubes.

In Fig. 2 we show the Arrhenius plot of the ASR values. From these data, we obtain the values for the activation energy (Ea) in the ranges of 1.45–1.74 eV for the LSCF($y-2$) cathodes and 1.39–1.51 eV for the LSCF($y-8$) cathodes. Those values are in close agreement with the values obtained previously for LSCO cathodes of similar characteristics [10,11]. We also see that, in agreement with previous data measured on LSC, the best electrochemical performance is

displayed by the cathodes made using membranes of smaller pore size (200 nm) that exhibited rod-like nanostructure.

3.1. Influence of the microstructure and composition at atmospheric pressure

From data of Figs. 1 and 2, we can observe the influence of the microstructure of the precursors on the electrochemical performance. We can see that cathodes with rod nanostructure present the lower ASR values. This result is very clear for $y=0.2$ and $y=0.8$, whereas for $y=0.5$ this feature, although present, is less significant. In particular, cathodes with rod nanostructure display promising values of ASR of the order of 0.1–0.2 Ω cm^2 for $T=700$ °C, a temperature usually considered as "intermediate-temperature".

In Table 2, we show the values for the activation energy (E_a) and ASR at 500 and 750 °C, measured in air, for all cathodes.

In all of the cases, cathodes made with nanostructured tubes of 200 nm display the best electrochemical performance. We have observed a similar behavior in a previous work performed on LSCO cathodes [11]. We showed that this result is a consequence of the morphology of the cathodes. The rods of the LSCF($y-2$) cathode expose a larger surface area compared with the tubes of the LSCF($y-8$) cathode. We observed that the whole diameter of the rods that arise from 200 nm diameter membranes, approximately fits into the walls of the tubes that result in the cathode made with 800 nm ones. A schematic picture is shown in Figure 9 of reference [11] that illustrates this idea. Consequently, LSCF($y-2$) cathodes exhibit a larger number of active sites for the oxygen reduction reaction and thus a better performance.

A comparison of the results for cathodes made with different precursors (Fig. 1) shows that the low frequency process, clearly observed for LSCFO($y-2$) cathodes, appears to be less significant in the LSCFO($y-8$) ones. A possible reason for this behavior is the following: the low frequency process is likely to be related with gas phase diffusion of oxygen [28] and represents a slight contribution to the overall EIS spectra measured in air; thus, its relative influence is expected to be more significant for the cathode in which all additional contributions are improved, which in our case are those with rod-like nanostructure.

Fig. 3 depicts the dependence of ASR with composition for LSCF($y-2$) and LSCF($y-8$) at 750 °C and 600 °C. We see that, in the case of LSCF($y-2$), cathodes with $y=0.2$ and 0.8 display similar ASR values and show better performance when compared with $y=0.5$. In contrast, for LSCF($y-8$), a monotonous decay in the performance is obtained when increasing Fe content (y).

3.2. Influence of the oxygen partial pressure: oxide-ion conduction and gas phase diffusion

Fig. 1(a) and (b) shows that the appearance of low frequency process whose relative influence depends on the type of nanostructure, being more significant in the LSCF($y-2$) cathodes formed by nanorods. To gain further insight on this behavior, we performed measurements in different $p(O_2)$. In Figs. 4 and 5, we show the EIS spectra at 500 °C and 750 °C for LSCF($y-2$) and LSCF($y-8$), respectively, with the measurements performed at $p(O_2)=0.05$, 0.21 and 1 atm. In all of the samples, the low frequency process becomes more evident at high temperature and low $p(O_2)$. In addition this

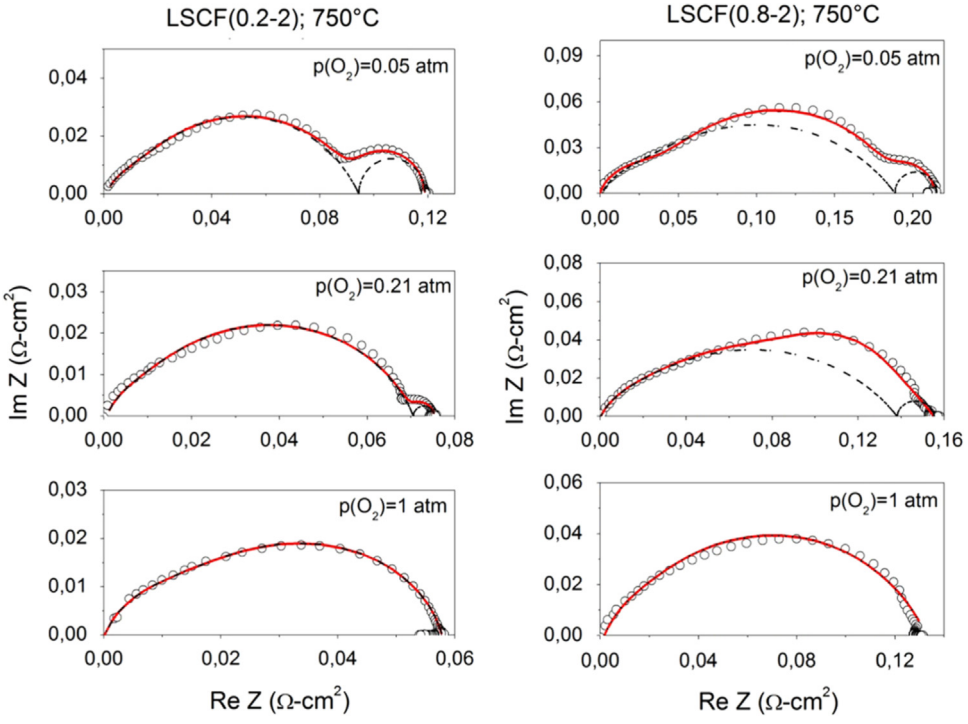

Fig. 6. Normalized Nyquist plots for [LSCF(0.2–2)/GDC/LSCF(0.2–2)] and [LSCF(0.2–8)/GDC/LSCF(0.2–8)] symmetric cells measured at 750 °C (open circles). $p(O_2)$ values of 1 atm, 0.21 atm and 0.05 atm are indicated in each graph. Fitting curves are shown in solid lines.

process is found to be much more significant for the LSCF ($y-2$) cathodes than for the LSCF($y-8$) cathodes, a fact that is clear, even at atmospheric pressure ($p(O_2)=0.21$). All compositions display a similar behavior.

As a reference, the ASR values for LSCF(0.2–2) and LSCF(0.2–8) cathodes, measured in different $p(O_2)$, are presented in Table 3.

We see that the improved performance of cathodes with rod nanostructure, previously observed at atmospheric pressure, is repeated for all atmospheres. As mentioned above, this result is probably related to the greater surface area of these cathodes formed by nanorods (and consequently a greater number of active sites for the oxygen reduction reaction) and to enhanced oxide-ion diffusion.

To independently analyze each of the contributions to the overall ASR, we modeled the EIS spectra using the following equivalent circuit shown in Fig. S4 of the Supplementary material [21]. We used a finite length Warburg element (Ws) in series with a parallel (R-CPE) element for the low frequency (LF) contribution to fit the data. A short explanation for each of the components can also be found on the Supplementary material [21]. The EIS spectra is characterized by a dominant finite length Warburg element, an indication of bulk diffusion, as is typical in MIEC conductors.

In Fig. 6, we present the fitting of the EIS data of LSCF(0.2–2) and LSCF(0.2–8) at 750 °C using the aforementioned model for the different values of $p(O_2)$.

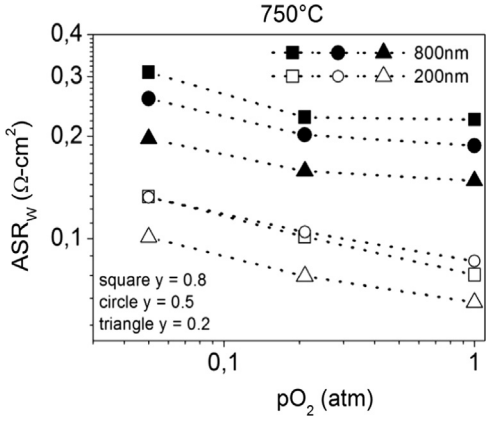

Fig. 7. ASR_W for LSCF($y-n$) cathodes at 750 °C (200 nm: rod-like nanostructure; 800 nm: tubular nanostructure).

We considered the low frequency process from the data and analyzed its resistive part (R_{LF}) as a function of oxygen partial pressure; the response is fitted by the following equation:

$$R_{LF} = = a(pO_2)^{-n} \quad (1)$$

with $n=1.1$, which is a signature of gas phase transport [29–32]. This result is also consistent with the appearance of the process on reducing $p(O_2)$ and its negligible contribution at atmospheric pressure. This last observation is expected behavior in MIEC conductors, in which there is no requirement for oxygen gas to travel and reach the triple phase boundary for oxygen reduction because the process can occur at the entire surface of the cathode.

In cathodes made with tubular nanostructure, the relative influence of the low frequency process is found to be less significant. This behavior is a consequence of the fact that, as observed in similar samples, in the cathodes made with nanorods, all of the other processes that contribute to the electrochemical properties (charge transfer, dissociative adsorption and bulk diffusion) are optimized, and thus, the appearance of gas phase diffusion at low $p(O_2)$ is more evident.

The intermediate frequency process, modeled with a finite length Warburg element, was extracted from the data to analyze its dependence with composition, morphology and $p(O_2)$.

In Fig. 7, we show the $p(O_2)$ dependence of the resistive part of the Warburg element (ASR_W) at 750 °C.

As a first observation, ASR_W is improved for cathodes with rod nanostructure. Additionally, a reduction of its value is observed while increasing $p(O_2)$. These first results are consistent with previously published results on LSC [11]. ASR_W can be fitted with

$$ASR_W = a(pO_2)^{-n} \quad (2)$$

with n values between 0.11 and 0.14. Such a small dependence is consistent with bulk diffusion through oxygen vacancies [33].

In the case of LSCF($y-2$) cathodes, an improved and similar performance is observed for $y=0.2$ and $y=0.8$, and for the LSCF($y-8$) cathodes, the performance increases monotonically from $y=0.8$ to $y=0.2$. Fig. 8 shows the dependences of the overall ASR and ASR_W with composition at different

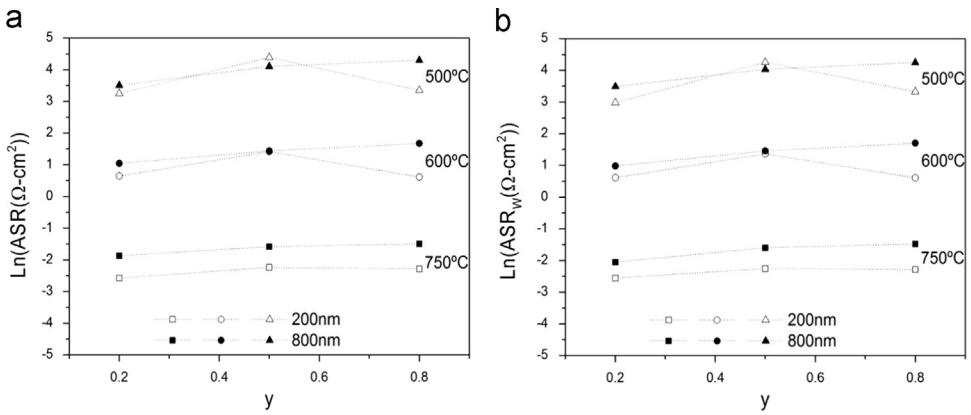

Fig. 8. (a) ASR and (b) ASR_W as a function of composition at 500, 600 and 750 °C.

temperatures measured in air. The behavior of the total ASR (Fig. 8a) and ASRw (Fig. 8b) is practically the same, which is to be expected, given the significant influence of bulk diffusion in the cathodic properties.

In all cases, cathodes made with nanorods display a better performance than those of tubular nanostructure. However, the dependence with composition is less significant because similar results were obtained for samples with different Fe contents. Samples with $y=0.2$ exhibited the best performance at 750 °C for both types of nanostructures.

Thus, the overall behavior revealed by our results clearly indicates that the electrochemical properties of the cathodes are highly influenced by the type of nanostructure whereas the influence of composition is not very important because no change of the chemical composition can compensate for the effect caused by the nanostructure.

4. Conclusions

In summary, we produced $La_{0.6}Sr_{0.4}Co_{1-y}Fe_yO_{3-\delta}$ nanostructured samples with $y=0.2$, 0.5, 0.8 by a pore wetting technique. Our nanostructures consist of an agglomeration of nanoparticles into the form of rods or tubes depending on the average pore size of the membrane. We used these precursors to produce nanostructured cathodes for SOFCs and studied their electrochemical properties in symmetrical cells.

The analysis of the Nyquist plots show a dominant Warburg process with small $p(O_2)$ dependence, which indicates that oxide-ion diffusion is the dominant process, as expected in MIEC cathodes. In agreement with our previous works for $La_{0.6}Sr_{0.4}CoO_3$, cathodes composed of nanorods display lower ASR values than cathodes composed of nanotubes if they are formed by nanoparticles of similar mean size. A small dependence with composition was also observed, but the influence of composition is much less significant compared with the effect produced by the nanostructure.

In conclusion, all of the materials considered display excellent properties for use as IT-SOFC cathodes. Therefore, the next step towards this direction is to test the performance of these materials in the operation of IT-SOFCs using different fuels. We are currently performing such a study and also comparing the performance of these nanomaterials with other nanomaterials, such as $La_{0.6}Sr_{0.4}CoO_3$ and $La_{0.8}Sr_{0.2}MnO_3$.

Acknowledgments

Financial support from CONICET (PIP00038), ANPCyT (PICT 1327, 1948 and 2689), MINCyT-CAPES cooperation agreement (Argentina-Brazil, project BR/11/red/02) and the Brazilian Synchrotron Light Laboratory (LNLS, under proposal XPD 10152) is acknowledged. The authors thank Manfredo H. Tabacniks and Marcia Fantini (Instituto de Física, USP, Brazil) for the RBS measurements and useful discussions, Adriana Domínguez, Gonzalo Zbihlei (CNEA, Argentina) and Mercedes Pianetti (INTI, Argentina) for SEM measurements and Solange di Napoli for the critical reading of the manuscript.

Appendix A. Supplementary material

Supplementary data associated with this article can be found in the online version at http://dx.doi.org/10.1016/j.ceramint.2015.10.104.

References

[1] S.C. Singhal, K Kendal, High-temperature solid oxide fuel cells: fundamentals, Des, Appl., Elsevier (2003).
[2] D.J.L. Brett, A. Atkinson, N.P. Brandon, S.J. Skinner, Intermediate temperature solid oxide fuel cells, Chem. Soc. Rev. 37 (2008) 1568.
[3] B. Sorensen, Fuel cells: optimism gone – hard work still there, Int. J. Hydrog.Energy 38 (2013) 7578–7582.
[4] U. Lucia, Overview on fuel cells, Renew. Sustain.Rev 30 (2014) 164–169.
[5] M.L. Perry, T.F. Fuller., A historical perspective of fuel cell technology in the 20th century, J. Electrochem. Soc. 149 (2002) S59–S67.
[6] J. Chen., A review of nanostructured lithium ion battery materials via low temperature synthesis, Recent Pat. Nanotechnol 7 (2013) 2–12.
[7] A.A. Balandin, Thermal properties of graphene and nanostructured carbon materials, Nat. Mater. 10 (2011) 569–581.
[8] Y. Wang, G. Cao, Developments in nanostructured cathode materials for high-performance lithium-ion batteries, Adv. Mater. 20 (2008) 2251–2269.
[9] L. Acuña, J. Peña-Martínez, D. Marrero-López, R. Fuentes, P. Nuñez, D. G. Lamas, Electrochemical performance of nanostructured $La_{0.6}Sr_{0.4}CoO_{3-\delta}$ and $Sm_{0.5}Sr_{0.5}CoO_{3-\delta}$ cathodes for IT-SOFCs, J. Power Sources 196 (2011) 9276–9283.
[10] M.G. Bellino, J. Sacanell, D.G. Lamas, A.G. Leyva, N.E. Walsoe de Reca, High-performance solid-oxide fuel cell cathodes based on cobaltite nanotubes, J. Am. Chem. Soc. 129 (2007) 3066–3067.
[11] J. Sacanell, A.G. Leyva, M.G. Bellino, D.G. Lamas, Nanotubes of rare earth cobalt oxides for cathodes of intermediate-temperature solid oxide fuel cells, J. Power Sources. 195 (2010) 1786–1792.
[12] F. Napolitano, A.L. Soldati, G. Jochen, D.G. Lamas, A. Serquis, Electronic and structural properties of $La_{0.4}Sr_{0.6}Ti_{1-y}Co_yO_{3\pm\delta}$ electrode materials for symmetric SOFC studied by hard X-ray absorption spectroscopy, Int. J, Hydrog. Energy 38 (2013) 8965–8973.
[13] A. Serquis, X.Z. Liao, Jy Huang, Q.X. Jia, D.E. Peterson, Y.T. Zhu, Co–Mo catalyzed growth of multi-wall carbon nanotubes from CO decomposition, Carbon 41 (13) (2003) 2635–2641.
[14] M.G. Zimicz, P. Nuñez, J. Ruiz-Morales, D.G. Lamas, S. Larrondo, Electro-catalytic performance of 60%NiO/Ce0.9Zr0.1O2 cermets as anodes of intermediate temperature solid oxide fuel cells, J. Power Sources 238 (2013) 87–94.
[15] M.G. Bellino, D.G. Lamas, N.E. Walsöe de Reca, Enhanced ionic conductivity in nanostructured, heavily doped ceria ceramics, Adv. Funct. Mater. 16 (2006) 107–113.
[16] M.G. Bellino, D.G. Lamas, N.E. Walsöe de Reca, A Mechanism for the fast ionic transport in nanostructured oxide-ion solid electrolytes, Adv. Mater. 18 (2006) 3005–3009.
[17] P.M. Abdala, G.S. Custo, D.G. Lamas, Enhanced ionic transport in fine-grained scandia-stabilized zirconia ceramics, J. Power Sources 195 (2010) 3402–3406.
[18] S. Boulineau, J.-M. Tarascon, J.-B. Leriche, V. Viallet., Solid State Ion 242 (2013) 45–48.
[19] J.M. Tarascon, D. Guyomard, G.L. Baker, An update of the Li metal-free rechargeable battery based on $Li_{1+\chi}Mn_2O_4$ cathodes and carbon anodes, J. Power Sources 44 (1993) 689–700.
[20] A.S. Aricó, P. Bruce, B. Scrosati, J.M. Tarascon, W. Van Schalkwijk, Nanostructured materials for advanced energy conversion and storage devices, Nat. Mater. 4 (2005) 366–377.
[21] See Supplementary material at [URL wil be inserted by AIP Publishing].

[22] P. Levy, A.G. Leyva, H.E. Troiani, R.D. Sánchez, Nanotubes of rare-earth manganese oxide, Appl. Phys. Lett. 83 (2003) 5247–5249.
[23] A.G. Leyva, P. Stoliar, M. Rosenbusch, V. Lorenzo, P. Levy, C. Albonetti, M. Cavallini, F. Biscarini, H. Troiani, J. Curiale, R. D. Sanchez, Microwave assisted synthesis of manganese mixed oxide nanostructures using plastic templates, J. Solid State Chem. 177 (2004) 3949–3953.
[24] D. Zhu, H. Zhu, Y.H. Zhang, Hydrothermal synthesis of single-crystal $La_{0.5}Sr_{0.5}MnO_3$ nanowire under mild conditions, J. Phys.: Condens. Matter 14 (2002) L519–L524.
[25] L. Hueso, N. Mathur, Nanotechnology: dreams of a hollow future, Nature 427 (2004) 301–304.
[26] S.J. Skinner, Recent advances in perovskite-type materials for SOFC cathodes, Fuel Cells Bull 4 (2001) 6–12.
[27] S. Adler, Mechanism and kinetics of oxygen reduction on porous $La_{1-x}Sr_xCoO_{3-\delta}$ electrodes, Solid State Ion 111 (1998) 125–134.
[28] J. Sacanell, M. Bellino, D.G. Lamas, A.G. Leyva, Synthesis and characterization $La_{0.6}Sr_0CoO_3$ and $La_{0.6}Sr_{0.4}Co_{0.2}Fe_{0.8}O_3$ nanotubes for cathode of solid-oxide fuel cells, Phys. B: Condens. Matter 398 (2007) 341–343.
[29] A. Ringuede, J. Fouletier, Oxygen reaction on strontium-doped lanthanum cobaltite dense electrodes at intermediate temperatures, Solid State Ion 139 (2001) 167–177.
[30] E.P. Murray, T. Tsai, S.A. Barnett, Oxygen transfer processes in (La,Sr)MnO_3/Y_2O_3-stabilized ZrO_2 cathodes: an impedance spectroscopy study, Solid State Ion 110 (1998) 235–243.
[31] E.C. Thomsen, G.W. Coffey, L.R. Pederson, O.A. Marina, Performance of lanthanum strontium manganite electrodes at high pressure, J. Power Sour 191 (2009) 217–224.
[32] S.R. Gamble, J.T.S. Irvine, 8YSZ/$(La_{0.8}Sr_{0.2})_{0.95}MnO_{3-\delta}$ cathode performance at 1–3 bar oxygen pressures, Solid State Ion 192 (2011) 394–397.
[33] A. Esquirol, N.P. Brandon, J.A. Kilner, M. Mogensen, Electrochemical characterization of $La_{0.6}Sr_{0.4}Co_{0.2}Fe_{0.8}O_3$ cathodes for intermediate-temperature SOFCs, J. Electrochem. Soc. 151 (2004) A1847–A1855.